Università degli Studi di Cagliari

Facoltà di Scienze Matematiche, Fisiche e Naturali

Laurea Magistrale in Fisica

Observation-Guided Simulation of the Extragalactic Binary Gravitational Wave Foreground in View of LISA

Relatore:

Prof. Riccardo Murgia

Co-relatori:

Prof. Thomas Kupfer
Weitian Yu

Candidato:

Gabriele Todde

ANNO ACCADEMICO 2024/2025

Indice

Introduction

In the context of the gravitational waves study, there are mainly two possible paths: the first is the **analysis of existing data** from experiments like Ligo, Virgo and Kagra, with the goal of detecting and characterizing the observable sources within their relative frequency bands; the second approach is the **forecasting approach**, which aims to characterize future experiments in order to better understand what types of sources they could detect and how well.

One of the most important future detectors is the European *Laser Interferometer Space Antenna* (LISA), the first space-based gravitational wave detector. LISA will be arranged as an equilateral triangle with 2.5 million kilometers long arms, placed in a heliocentric orbit, and will operate within the frequency range from approximately 0.1mHz to 1Hz. Among the typical sources that emit gravitational wave signal in this range are the **compact binaries**, and in our particular case we are interested in **double white dwarf binaries** (**WDBs**).

The goal of this work is to estimate the gravitational wave background produced by the extragalactic WDBs in the local universe, by using the **COSMIC** code to generate synthetic astrophysical populations to represent the galaxies listed in the **Gravitational Wave Galaxy Catalog** (**GWGC**).

In **Chapter 1** we will introduce the theoretical foundations of gravitational waves, derive the amplitude of the signal generated by a binary system, and define the most important parameters. Finally, we discuss how to combine the signals from multiple sources, to find a cumulative background.

In **Chapter 2** we will give a brief overview of how gravitational wave detectors work, trying to better understand what kinds of sources LISA will be able to see, what resolution and what sensitivity it will have and why in particular we are interested in WDBs.

In **Chapter 3** we introduce the concept of stellar population synthesis and the code COSMIC used for this purpose. We will introduce its features, main parameters, and pipeline, and explain how it is used to generate full-size astrophysical populations of WDBs.

In **Chapter 4** we introduce the GWGC, list the key information it provides and explain how we move from there to infer the remaining parameters that we need.

In **Chapter 5** we use the obtained information to compute the total gravitational wave signal summing the contribution from all the simulated sources, taking into account their spatial distribution, LISA's frequency resolution, and the *zone of avoidance* caused by the milky way.

In **Chapter 6** we plot the total resulting signal on the LISA sensitivity curve, and discuss the results and their possible implications.

Finally, in **Chapter 7** we will draw some conclusions from the work as a whole, discussing its limitations, assumptions and its possible extensions and follow-ups.

Capitolo 1

Theoretical Framework

1.1 Gravitational Waves Theory

After considering, in 1905, the problem of the apparently *instantaneous* propagation of light, with the theory of Special Relativity, in 1916 Albert Einstein considered the problem of the apparently *instantaneous* propagation of gravity through *long distances*, in his theory of General Relativity. Einstein showed that long-distance interaction arises from the deformation of space time caused by massive objects. Hence, in the "static case", the deviated motion apparently caused by the interaction between two distant masses really is, in fact, a manifestation of space time curvature nearby, generated by the presence of the two objects. The "static case" just depicted, though, treats the curvature as if it had always been there, and doesn't take into account of any variation in the masses, positions or velocities of the two objects, that would induce an evolution to the curvature itself. In truth, after a change in the mass-energy distribution, the corresponding curvature variation requires its time to reach far distances, and a fascinating prediction of General Relativity is that it propagates in the form of a wave, that travels at the speed of light.

1.1.1 Gravitational Waves as Perturbations

The typical approach to the study of gravitational waves is to derive them as small perturbations of the background from the Einstein's equations:

$$G_{\mu\nu} = R_{\mu\nu} - \frac{1}{2}g_{\mu\nu}R, \tag{1.1}$$

which can be conveniently written as

$$R_{\mu\nu} = \frac{8\pi G}{c^4}\left(T_{\mu\nu} - \frac{1}{2}g_{\mu\nu}T\right), \tag{1.2}$$

where $G_{\mu\nu}$ is the Einstein tensor, $R_{\mu\nu}$ is the Ricci tensor, R is the Ricci scalar, $g_{\mu\nu}$ is the metric of space time, and $T_{\mu\nu}$ is the stress-energy tensor. As a background solution we can consider the flat space time described by the metric $\eta_{\mu\nu}$, to which the perturbation term appears as a fluctuation in the metric $|h_{\mu\nu}| \ll |\eta_{\mu\nu}|$, known as *weak field* approximation. Thus, the perturbed space time can be written as:

$$g_{\mu\nu} = \eta_{\mu\nu} + h_{\mu\nu}, \qquad |h_{\mu\nu}| \ll |\eta_{\mu\nu}|.$$

With this metric, the equations 1.2 becomes

$$\{\Box_F h_{\mu\nu} - \left[\frac{\partial^2}{\partial x^\lambda \partial x^\mu} h^\lambda_\nu + \frac{\partial^2}{\partial x^\lambda \partial x^\nu} h^\lambda_\mu + \frac{\partial^2}{\partial x^\nu \partial x^\mu} h^\lambda_\lambda\right]\} = -\frac{16\pi G}{c^4}\left(T_{\mu\nu} - \frac{1}{2}\eta_{\mu\nu}T\right).$$

Now, by requiring that the *weak-field* approximation remains satisfied for infinitesimal diffeomorphisms, and by choosing a coordinate system in which the *harmonic gauge condition*[1], defined as

$$\Gamma^\lambda = g^{\mu\nu}\Gamma^\lambda_{\mu\nu} = 0, \tag{1.3}$$

where $\Gamma^\lambda_{\mu\nu}$ are the *affine connections*, is satisfied, we can find that, up to first order in $h_{\mu\nu}$, the harmonic gauge condition is equivalent to

$$\frac{\partial}{\partial x^\mu} h^\mu_\rho = \frac{1}{2}\frac{\partial}{\partial x^\rho} h, \qquad h = \eta^{\mu\nu} h_{\mu\nu} \equiv h^\nu_\nu. \tag{1.4}$$

After defining the *trace-reversed*[2] tensor as

$$\bar{h}_{\mu\nu} \equiv h_{\nu\mu} - \frac{1}{2}\eta_{\mu\nu} h,$$

we can finally write the linearized Einstein equations as

$$\begin{cases} \Box \bar{h}_{\mu\nu} = -\frac{16\pi G}{c^4} T_{\mu\nu}, \\ \partial^\mu \bar{h}_{\mu\nu} = 0. \end{cases}$$

This form, and its twin with $T_{\mu\nu} = 0$, where the first equation becomes the D'Alambert equation, are relevant because they show that *a perturbation of a flat space time propagates as a wave travelling at the speed of light*. As in Electrodynamics, the solution of (1.5) can be written in terms of *retarded potentials*:

$$\bar{h}_{\mu\nu}(t, \mathrm{x}) = \frac{4G}{c^4}\int_V \frac{T_{\mu\nu}(t - \frac{|\mathrm{x}-\mathrm{x}'|}{c}, \mathrm{x}')}{|\mathrm{x}-\mathrm{x}'|} d^3x', \tag{1.5}$$

where V is the three dimensional source volume, x' is the distance of an element of the emitting source from the origin of a frame centered in the same point of the source, x is the distance between source and observer. It can be proved that the solutions in (1.5) automatically satisfy the harmonic gauge condition in the second equation of the (1.5).

Harmonic gauge

It is important to notice that if the *harmonic gauge* condition is not satisfied in a reference frame, a new frame in which it is can always be found, by making an infinitesimal coordinate transformation

$$x^{\lambda'} = x^\lambda + \epsilon^\lambda, \tag{1.6}$$

[1]It is an arbitrary coordinate condition which makes it possible to solve the Einstein field equations. It can be found by requiring that the linearized Einstein equations satisfy the D'Alambert equation.

[2]The name comes by noting that $\bar{h} = \eta^{\mu\nu}\bar{h}_{\mu\nu} = -h$.

provded that ϵ^λ satisfies the following equation:

$$\Box_F \epsilon_\rho = \frac{\partial h^\beta_\rho}{\partial x^\beta} - \frac{1}{2}\frac{\partial h}{\partial x^\rho} = 0\ .$$

This is an inhomogeneous wave equation that can be solved to find the components ϵ_α, which identify the coordinate system in which the harmonic gauge condition is satisfied. Notice though, that the harmonic condition in (1.3) does not determine the gauge uniquely, but instead leaves some more gauge freedom to be used.

1.1.2 The physical wave

As we have seen, perturbations of flat space-time satisfy a wave equation and a harmonic gauge condition, as in (1.5). The general solutions of these wave equation is a linear superposition of monochromatic plane waves, with a polarization tensor (or wave amplitude) $A_{\mu\nu}$ and a wave four-vector $\vec{k}$, such as

$$\Box_F \bar{h}\mu\nu = -A_{\mu\nu}\eta^{\alpha\beta}k_\alpha k_\beta e^{ik_\gamma x^\gamma} = 0.$$

Thus, neglecting the trivial solution $A_{\mu\nu} = 0$, gives

$$\eta^{\alpha\beta}k_\alpha k_\beta = 0,$$

which means that $\vec{k}$ is a null vector. If we also consider the harmonic gauge, we find a condition that imposes the orthogonality of the wave four-vector to the polarization tensor,

$$k_\mu A^\mu_\nu = 0.$$

The *wavefronts*, i.e. the spatial surfaces where $\bar{h}_{\mu\nu} = const.$ are the planes where $k_i x^i = const.$ Conventionally, k^0 is referred to as $\frac{\omega}{c}$, where ω is the frequency, thus

$$\vec{k}_0 = \left(\frac{\omega}{c}, \mathbf{k}\right),$$

where $\mathbf{k}$ is the wave three-vector orthogonal to the wavefront, and is related to the *wavelenght* by $|\mathbf{k}| = 2\pi/\lambda$. Notice that, since the wave four-vector $\vec{k}$ is a null vector, it follows that

$$-(k^0)^2 + |\mathbf{k}| = 0 \rightarrow \omega = ck_0 = c|\mathbf{k}|,$$

which gives the dispersion relation for a wave moving at the speed of light.

The TT gauge

In a one dimension case, the wave equation can be written as

$$\left(-\frac{1}{c^2}\frac{\partial^2}{\partial t^2} + \frac{\partial^2}{\partial x^2}\right)\bar{h}^\mu_\nu = 0,$$

which generally has, as solution, an arbitrary function of $t \pm \frac{x}{c}$. If we consider, for example, a progressive wave $\bar{h}^\mu_\nu[f(t,x)]$, where $f(t,x) = t - \frac{x}{c}$, and apply the harmonic gauge condition, focusing only in the time-depndent part of the solution, we find the *first four* conditions:

$$\bar{h}^t_t = \bar{h}^x_t, \quad \bar{h}^t_x = \bar{h}^x_x, \quad \bar{h}^t_y = \bar{h}^x_y, \quad \bar{h}^t_z = \bar{h}^x_z. \tag{1.7}$$

As we have already discussed, there still is the freedom of making an infinitesimal coordinate change, and by requiring that the harmonic gauge remains satisfied in the new coordinates generates *four more conditions*:

$$\bar{h}^t_x = \bar{h}^t_y = \bar{h}^t_z = \bar{h}^y_y + \bar{h}^z_z = 0, \tag{1.8}$$

and with the (1.7) follows

$$\bar{h}^x_x = \bar{h}^x_y = \bar{h}^x_z = \bar{h}^t_t = 0.$$

The only non zero components are $\bar{h}^z_y$ and $\bar{h}^y_y - \bar{h}^z_z$, which cannot be set to zero because now we have completely used all the gauge freedom. It can be shown that, from all the above conditions, it follows that $\bar{h} \equiv h$, i.e. in this gauge the wave results to be *traceless*. Thus, a plane gravitational wave propagating along the x-axis is characterized by only two non-zero functions h_{zy} and $h_{yy} = -h_{zz}$:

$$h^{TT}_{\mu\nu} = \begin{pmatrix} 0 & 0 & 0 & 0 \\ 0 & 0 & 0 & 0 \\ 0 & 0 & h_{yy} & h_{yz} \\ 0 & 0 & h_{yz} & -h_{yy} \end{pmatrix}. \tag{1.9}$$

In conclusion, the gravitational wave only has **two physical degrees of freedom** which correspond to two polarization states. This gauge is called **TT gauge** because of the *transverse traceless* nature: $h_{\mu\nu}$ is traceless, thus $h = 0$, and transverse, since the components of $h_{\mu\nu}$ along the direction of propagation are null (in this case $h_{\mu_x} = 0$).

1.1.3 Motion and geodesics

Free test particles in General Relativity move along geodesic, which means that, in terms of a world line $x^\mu(\tau)$ parametrized by proper time τ, they satisfy the *geodesic equation*:

$$\frac{d^2x^\alpha}{d\tau^2} + \Gamma^\alpha_{\mu\nu}\frac{dx^\mu}{d\tau}\frac{dx^\nu}{d\tau} \equiv \frac{du^\alpha}{d\tau} + \Gamma^\alpha_{\mu\nu}u^\mu u^\nu = 0, \tag{1.10}$$

where $u^\alpha = \frac{dx^\alpha}{d\tau}$ is the particle velocity. By imposing the rest condition, $u^\alpha = (1, 0, 0, 0)$, to the (1.10) and considering the TT gauge component prescriptions for $h_{\mu\nu}$, we find that a particle initially at rest is not accelerated by the passage of a wave, but remains at a fixed coordinate position: the motion of a single particle is not affected by the gravitational waves.

The geodesic deviation

If we consider, instead, the relative motion of close particles, the situation is different. This relative motion is governed by the *geodesic deviation*, which quantifies how two very close geodesics deviate from one another. Although, as we have seen, the coordinates of the two particles (and thus their difference) do not change when a gravitational wave passes, this does not hold true for their *proper distance* o

$$\Delta l = \int ds \neq const.$$

This apparent contradiction arises from the fact that the coordinate difference is not a *tensorial* quantity, and therefore is not suited to describe properly a physical process. This is the reason we consider the geodesic deviation, which provides a tensorial formulation of the relative acceleration between the two particles:

$$\frac{D^2 \delta x^\alpha}{d\tau^2} \equiv (\Delta_{\vec{t}}(\Delta_{\vec{t}}\vec{\delta x}))^\alpha = R^\alpha_{\beta\mu\nu} t^\beta t^\mu \delta x^\nu, \tag{1.11}$$

where

$$R_{\alpha k \lambda \mu} = \frac{1}{2}(g_{\alpha\mu,\lambda k} + g_{k\lambda,\mu\alpha} - g_{\alpha\lambda,\mu k} - g_{k\mu,\lambda\alpha}) \tag{1.12}$$

is the Riemann curvature tensor, $\vec{t}$ is the tangent vector to one of the geodesic, and $\vec{\delta x}$ is a deviation vector between the two geodesics. it is important to note that in the presence of a gravitational wave the Riemann tensor is never zero in any reference frame, and consequently neither is the geodesic deviation. In contrast, the quantity $\frac{d^2 \delta x^i}{d\tau^2}$ (which is not a tensorial quantity) vanishes in the TT frame.

Knowing this, to analyze this effect in more detail we can choose to integrate the (1.11) in a *Locally Inertial Frame*, LIF $\{\xi^\alpha\}$, centered on one of the two particles, where the metric can be approximated close to the origin as Minkowski up to quadratic, negligible, corrections:

$$ds^2 = \eta_{\alpha\beta} d\xi^\alpha d\xi^\beta + O(|\xi|^2).$$

In this frame, the Riemann tensor in (1.12), which depends on second derivatives of the metric perturbation $h_{\mu\nu}$ (with $g_{\mu\nu} = \eta_{\mu\nu} + h_{\mu\nu}$), is not only covariant, but actually *invariant* under infinitesimal coordinate transformations from a generic LIF to the TT frame. This is especially useful because in the TT frame $h^{TT}_{\mu\nu}$ takes a particularly simple form, as we have seen in the (1.9) example, simplifying also the expression for $R^{TT}_{\alpha k \lambda \mu}$. Assuming that the wave travels along the ξ^1 direction, the solutions for the geodesic deviation equation for two close particles are the non zero components of

$$\delta\xi^j = \delta\xi^j_0 + \frac{1}{2}\eta^{ji} h^{TT}_{ik} \delta\xi^k_0, \tag{1.13}$$

where $\delta\xi^j_0$ represent the initial, constant separaion between the particles. As previously discussed, the non-zero components of the strain tensor h^{TT}_{ik} correspond to two possible polarizations of the gravitational wave. Their distinct effects on a ring of close particles are viually represented in **Figure 1.1**.

1.1.4 The Quadrupole Approximation

Now that we have discussed the effects of the passage of a gravitational wave on the relative motion of close particles, we can focus on another important ptoblem: *how*

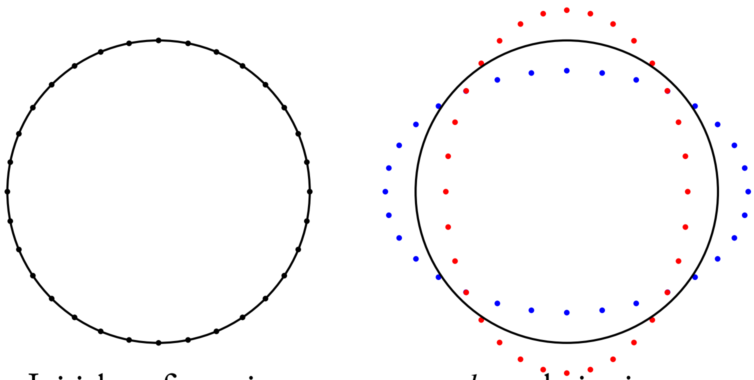

Figura 1.1: Effect of the two gravitational wave polarizations on a ring of free-falling particles: blue and red dots represent two opposite phases of the wave.

such waves are generated. Gravitational radiation is a consequence of variations in the spacetime curvature, and it generates from time-dependent distributions of mass and momentum. But not every motion of matter can produce gravitational wave signal, as we will see: conservation laws of general relativity, impose strict constraints on the possible multipole moment that can contribute to the tensorial metric perturbations.

The weak-field, slow-motion approximation

We already introduced previously the weak-field limit, which allows us to write the metric as a perturbed Minkowski $g_{\mu\nu} = \eta_{\mu\nu} + h_{\mu\nu}$, with $|h_{\mu\nu}| \ll 1$, and we found the solutions as in (1.5). Until now, we have only solved these equations with a null stress-energy tensor. If we assume that the region, of size ϵ, where the source of the signal is confined, is much smaller than the wavelenght of the emitted gravitational radiation, $\lambda_{GW} = \frac{2\pi c}{\omega}$, we find the following condition:

$$\frac{2\pi c}{\omega} \gg \epsilon \rightarrow \epsilon\omega \ll c \rightarrow v_{typical} \ll c. \tag{1.14}$$

The typical velocities of the system are much smaller than the speed of light: this is the so called *slow motion approximation*. If we now use the solution found using the retarded potentials in (1.5), by making use of the Fourier transforms it can be found that the gravitational wave signal emitted by the source, to leading order in the weak-field, slow-motion approximation is

$$\bar{h}_{\mu\nu}(t,r) = \frac{4G}{rc^4}\int_V T_{\mu\nu}(t - \frac{r}{c}, \mathrm{x}')d^3x. \tag{1.15}$$

The quadrupole formula

The integral in (1.15) can be simplified with some expedients. First of all, by making use of the conservation law that applies to the stress-energy tensor

$$\frac{\partial T^{\mu\nu}}{\partial x^\nu} = 0, \quad \rightarrow \quad \frac{1}{c}\frac{\partial T^{\mu 0}}{\partial t} = -\frac{\partial T^{\mu\nu}}{\partial x^k}, \quad \mu = 0, \ldots, 3, \;\; k = 1, 2, 3,$$

a smart use of the Gauss' theorem (reminding that the stress-energy tensor is null on the source's surface), it can be found that

$$\bar{h}^{\mu\nu} = 0.$$

Secondly, we can use the **tensor-virial theorem**

$$\frac{1}{c^2}\frac{\partial^2}{\partial t^2}\int_V T^{00}x^k x^n d^3x = 2\int_V T^{kn} d^3x, \quad k,n = 1,2,3, \tag{1.16}$$

in the definition of the **quadrupole moment tensor**

$$q^{kn}(t) = \frac{1}{c^2}\int_V T^{00}(t,\mathrm{x})x^k x^n d^3x, \tag{1.17}$$

we finally find that (1.15) can be re-written as

$$\begin{aligned} &\bar{h}^{\mu 0} = 0, \\ &\bar{h}^{ik}(t,r) = \frac{2G}{c^4 r}\frac{d^2}{dt^2}q^{ik}(t-\frac{r}{c}), \end{aligned} \tag{1.18}$$

known as the **quadrupole formula.** This formulation describes the gravitational wave signal emitted by a gravitating system that evolves in time, whatever the mass-energy distribution looks like, as long as $\ddot{q}^{ik} \neq 0$. Note that in this approximation, the only component of the stress-energy tensor that generates the metric perturbation is T^{00}, and that the c^{-4} rendes the characteristic strain extremely small:

$$\frac{G}{c^4} \sim 10^{-49}\frac{s^2}{g\ cm}.$$

Transform to the TT gauge

The solution in (1.18) represents a spherical wave far from the source, which locally looks like a plane wave. It can also be expressed, after an infinitesimal coordinate trasformation that preserves the harmonic gauge. This projection in the TT gauge is performed by defining symmetric and transverse *projector operators* as

$$P_{jk} \equiv \delta_{jk} - n_j n_k,$$

to than define the **transverse-traceless projector**

$$P_{jkmn} \equiv P_{jm}P_{kn} - \frac{1}{2}P_{jk}P_{mn}, \tag{1.19}$$

which "extracts" the transverse-traceless part of a rank two tensor on the three-dimensional Euclidean space. This way we can, for example, define

$$h^{TT}_{jk} = P_{jkmn}\bar{h}_{mn},$$

that, if applied to the (1.18), gives

$$\bar{h}^{TT}_{\mu 0} = 0,$$
$$\bar{h}^{TT}_{ik}(t,r) = \frac{2G}{c^4 r}\frac{d^2}{dt^2}Q^{TT}_{ik}(t-\frac{r}{c}), \tag{1.20}$$

where $Q^{TT}_{jk} = P_{jkmn}q_{mn}$ is the **transverse-traceless part of the quadrupole moment.** As we will see, to compute the "luminosity" of a gravitational wave source, it is useful to define the **reduced quadrupole moment**

$$Q_{jk} \equiv q_{jk} - \frac{1}{3}\delta_{jk}q^m_m, \tag{1.21}$$

which is traceless by definition.

Gravitational waves from a binary system

As an example, we can consider a binary system where two masses m_1 and m_2 are in a circular orbit around the common center of mass. The typical parameters are the total mass

$$M \equiv m_1 + m_2,$$

the *reduced mass*

$$\mu \equiv \frac{m_1 m_2}{M},$$

and, by placing the origin of the coordinate frame in the center of mass,

$$l_0 = r_1 + r_2, \quad r_1 = \frac{m_2}{M}l_0, \quad r_2 = \frac{m_1}{M}l_0, \quad \omega_K = \sqrt{\frac{GM}{l_0^3}}.$$

Now, after defining the coordinates of the masses (x_1, y_1) and (x_2, y_2) in an orbital plane, orthogonal to the z-axis, as functions of all the above parameters, it becomes possible to compute the 00-component of the stress-energy tensor as

$$T^{00} = c^2 \sum_{n=1}^{2} m_n \delta(x - x_n)\delta(y - y_n)\delta(z),$$

and thus all the non-vanishing components of q_{jk}. From this we can find Q_{jk}, Q^{TT}_{jk}, and finally

$$h^{TT}_{ij}(t,r) = -\frac{A}{r}A^{TT}_{ij}(t-\frac{r}{c}), \tag{1.22}$$

where

$$A = \frac{4\mu M G^2}{l_0 c^4},$$
$$A^{TT}_{ij}(t-\frac{r}{c} = P_{ijkl}Akl(t-\frac{r}{c}), \tag{1.23}$$

and[3]

$$A_{\mu\nu}(t) = \begin{pmatrix} \cos 2\omega_K t & \sin 2\omega_K t & 0 \\ \sin 2\omega_K t & -\cos 2\omega_K t & 0 \\ 0 & 0 & 0 \end{pmatrix}.$$

Using typical values, such as the PSR 1913+16 assuming it had a circular orbit, by defining

$$h_0 = \frac{A}{r},$$

and using (1.23), we find

$$h_0 \sim 5 \times 10^{-23},$$

as an estimate of a typical gravitational wave signal amplitude generated by a binary system.

1.1.5 Energy carried by a gravitational wave

The stress-energy tensor conservation laws that we know in Special relativity

$$T^{\mu\nu}_{,\nu} = 0,$$

unfortunately do not hold in General Relativity. Indeed, the Stress-energy tensor describes the energy and momentum of the sources of the gravitational field, but not of the gravitational field itself: to have a proper conservation we would need to consider both contributions. The equivalence principle states that the effect of the gravitational field vanishes in a LIF centered on a particle; if there was a tensor describing it, it would be null in this frame too. But if a tensor field is null in one frame, than it must be in all the other too: for this reason, there cannot be anything like a true gravitational field tensor.

Stress-energy pseudo-tensor

For this reason, we are going to introduce a **stress-energy pseudo tensor**, where a pseudo-tensor is a mathematical object that behaves like a tensor only under linear coordinate transformations. It is possible to define procedures of *integration* or *averaging* involving it, which allow to construct well-defined gauge-invariant quantities. In particular, it is possible to define a *local* notion of energy and momentum in the weak field approximation, on the assumption that the characteristic length-scale λ of the perturbation is much smaller than the characteristic length-scale L of the background: $\lambda/K \ll 1$. In this regime, it can be shown that if averaged over multiple wavelengths λ, the stress-energy pseudo-tensor transforms as a tensor for coordinate transformations linear in h (i.e. of order $O(h)$),

$$\langle t^{\mu\nu} \rangle,$$

and is therefore *suitable to describe energy and momentum carried by the perturbation*.

[3]Note that this shows that a *binary system in circular orbits emits waves at twice the orbital frewuency*a

Gravitational wave luminosity

In general, it can be shown that the energy flowing across a unit surface orthogonal to the direction x' per unit time is given by the $0x'$ component of the stress-energy tensor times the speed of light. Similarly, the energy flux of a gravitational wave propagating in the same direction is given by the same component of the stress-energy pseudo-tensor averaged over several wavelengths, and can be derived as

$$\frac{dE_{GW}}{dtdS} = c\langle t^{0x'}\rangle = \frac{c^3}{16\pi G}\langle(\dot{h}_+(t,x'))^2 + (\dot{h}_x(t,x'))^2\rangle.$$

where h_+ and h_x are the analog of h_{yy} and h_{yz} in the (1.9), and represent the metric perturbation polarizations. In the TT frame, by directly substituting what we have found in (1.20), we find

$$\frac{dE_{GW}}{dtdS} = \frac{G}{8\pi c^5 r^2}\left\langle \sum_{jk}\left(\dddot{Q}^{TT}_{jk}(t-\frac{r}{c}\right)^2\right\rangle,$$

and after defining the **gravitational wave luminosity** as

$$L_{GW} = \frac{dE_{GW}}{dt} = \int \frac{dE_{GW}}{dtdS}dS,$$

and writing Q^{TT} as a function of (1.21), by using the TT projectors in (1.19) and their properties, it can be shown that the energy associated to a ravitational wave can be written as the **luminosity quadrupole formula:**

$$L_{GW}(t) = \frac{G}{5c^5}\left\langle\left(\dddot{Q}_{ij}(t-\frac{r}{c}\right)\left(\dddot{Q}_{ij}(t-\frac{r}{c}\right)\right\rangle, \tag{1.24}$$

as was derived by Einstein[4] in 1918.

1.1.6 Evolution of a compact binary system

Signal from inspiralling compact objects

Here we get to the actual amplitude we used, and the parameters involved.

1.2 White dwarfs and galaxies

1.2.1 White dwarfs

1.2.2 Galaxies

Morphological types

Here I introduce Hubble types, explaining general physical differences between them. Later I will introduce the T value notation and how to translate in the Hubble sequence types.

[4]insert the reference?

1.3 LISA

1.4 interferometers

- Instrument description (what is an interferometer, why in space, how it will be made, orbit) - frequency band - what will it see? - frequency resolution - sensibility curve and ASD meaning - Why WD choice in particular?

Capitolo 2

Methods and Data

The abundance of information of the electromagnetic spectrum allowed us to build highly detailed models of various celestial objects such as stars, both on their individual internal structure and on how this is influenced by the interaction with other bodies, for instance in binary systems. In the pursuit of reaching a greater sensitivity in the gravitational counterpart too, which could potentially reveal new information, or place better constrains on the existing models, these stellar models, when combined with a good theory of gravity, can be used to construct synthetic populations that reproduce observable features like luminosity, color, and chemical composition, which could enable us to predict what their gravitational signal would look like. In gravitational waves research, our observational capabilities are still very limited, and the signals are still comparatively very weak relative to their electromagnetic counterpart. Therefore, methods that rely on simulations can be very useful both to explore how different sources could look like in the gravitational wave domain, and how effectively they could be detected with current or future instruments.

2.1 Stellar populations synthesis codes

Generating a synthetic population of stars is a very complex task, that involves multiple steps, each involving important choices. *First*, we need to choose a starting point: we could start from the very beginning of stars formation and simulate all the process from the birth onward, or we could select a later phase in the stars evolution, shared from the most, in order to reduce unnecessary computational power and time consumption. If we want to simulate entire stellar populations choosing a starting point also implies selecting appropriate distributions for the main parameters that characterize the "starting point population", like masses, metallicities, but also orbital parameters for the stars that are in binary systems, like orbital period, distance, and eccentricity. *Second*, we must choose how the stars will evolve from the starting point, and this involves the single star evolution but also the effects that interaction with other stars in binary systems have on it. *Finally*, we have to decide when we want to stop the simulation, choosing an endpoint that aligns with the needs of this study.

2.1.1 The starting point

As we know, in the Hertzsprung-Russel diagram, which plots the *luminosity* of the stars vs their *color index*, most of the stars appear distributed in the **main sequence** (**MS**), a continuous and distinctive band. A star's position on this band is determined by its initial mass, and a good rule of thumb is that the most massive stars are hotter, more luminous, and evolve more quickly, while the lower-mass stars burn their fuel more slowly, and remain on the MS longer.

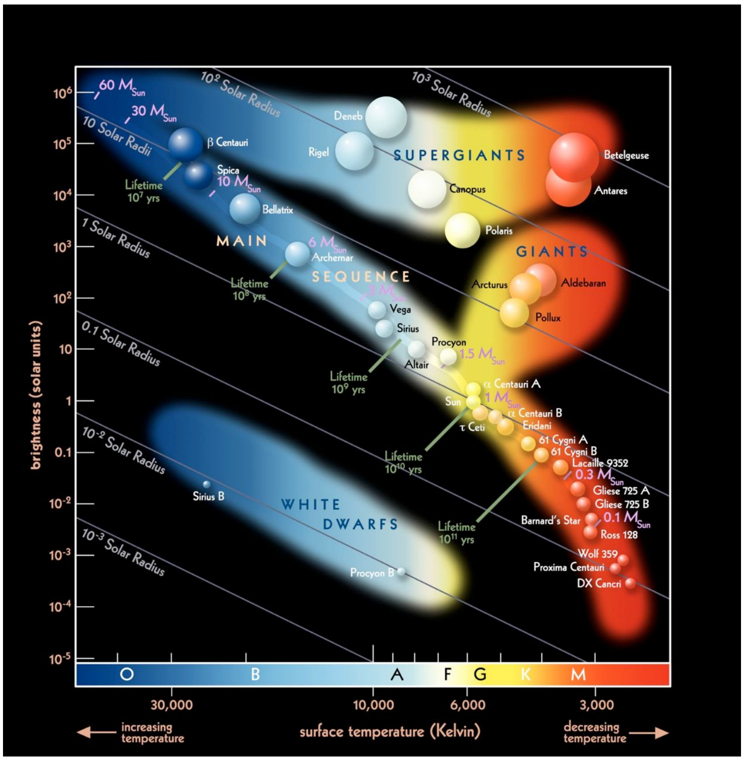

Figura 2.1: WRITE CAPTION, INSERT REFERENCE

Since almost all stars go through a phase in the MS, and evolve from there differently, in this work, the chosen starting point for stellar evolution is the Zero Age Main Sequence (ZAMS). At this stage, stars have just begun hydrogen burning in their cores, marking the start of their stable main sequence phase. This allows to bypass the early phases of star formation, which are much less relevant to the gravitational wave sources of interest, while still capturing the essential evolutionary processes that lead to the formation of compact objects.

2.1.2 Single star evolution

Simulating the evolution of a single star is in itself a very complex matter, and the only way to make it computationally feasible in the context of large-scale population synthesis is to approximate the evolution for a wide range of mass M and metallicity Z. In fact, detailed evolution codes can require substantial computational time even for the evolution of a single star, which is not practical when generating a full-scale astrophysical population containing millions of stars. Also, in order to make population synthesis statistically robust a large enough number of stars of a certain type must be evolved in order to overcome stochastic noise (in particular, the Poisson noise for n simulations of a particular type of star, implies an error that grows as $\sqrt{n}$). A winning strategy, adopted by several population synthesis frameworks, is to pre-generate a large grid of detailed stellar evolution models, and use them to derive a number of interpolation formulae as functions that approximate stellar properties as a function of age, mass and metallicity. In Hurley et al. [2000] this method is implemented through the development of a set of **Single Star Evolution** (**SSE**) formulae, with the result of a very compact, efficient and adaptable code, which makes it perfect for the integration of binary-star interactions. The work presented in Hurley et al. [2000] therefore serves as the theoretical and computational foundation for many complex stellar population synthesis codes, including the one used in this thesis. It takes care of the single-star evolution of stars from ZAMS through all the possible evolutionary outcomes, depending on the star's initial conditions.

2.1.3 Binary stars evolution

While the evolution of single stars already represents a challenge, the inclusion of binary interactions introduces a much higher level of complexity. In such systems, the evolution of each star is strongly influenced by its companion through a variety of processes, such as mass transfer and accretion, common envelope evolution, collisions, supernova kicks, tidal effects, angular momentum loss, and mergers. These interactions can drastically alter the final outcomes, and are essential for modeling the formation of compact binaries that are potential gravitational wave targets for LISA. To efficiently model binary evolution within the framework of stellar population synthesis, the work of Hurley et al. [2002] extends the SSE formalism by introducing a set of prescriptions for binary interactions, and updating the treatment of processes such as Roche lobe overflow, common envelope evolution ans coalescence by collision, leading to the development of the **Binary Star Evolution** (**BSE**) algorithm. This code includes the interpolation-based approach used in SSE for single-star evolution, but adds a comprehensive treatment of binary-specific processes, enabling the simulation of a wide range of binary configurations but keeping the affordable computational requirements of SSE. The BSE algorithm tracks the joint evolution of both stars in a binary system, taking into account their initial parameters, such as masses, orbital period, eccentricity, and metallicity, and updates these properties dynamically as the system evolves. The flexibility and speed of the BSE code make it a key component in many modern population synthesis tools, including the one used in this thesis, which we will now introduce.

2.2 COSMIC

For the purposes of this work, we employ a community-developed binary population synthesis (BPS) python-based code, called the **Compact Object Synthesis and Monte Carlo Investigation Code** (**COSMIC**), whose «*primary purpose is to generate synthetic populations with an adaptive size based on how the shape of binary parameter distribu-*

tions change as the number of simulated binaries increases» [1]. COSMIC's binary evolution is built upon BSE, incorporating extensive modifications in order to include updated physical prescriptions. It includes all necessary tools to generate a population, from the generation of initial conditions, to scaling the simulated systems to full-scale astrophysical populations. The code is presented in Breivik et al. [2020], where it is described in full detail and used, as a proof of concept, to simulate the Galactic population of compact binaries and their associated gravitational wave signal. In the following section we will see the main features of the code, and explain what makes it the right choice for this thesis work.

2.2.1 Fixed population

A fundamental concept in COSMIC, which is the key to the code's efficiency, is the idea of *fixed population*. This refers to a relatively small sample[2] of just enough binaries to capture, in a statistically meaningful way, the underlying shape of the parameter distribution functions of the target population, as determined by the user specified Star Formation History (SFH) and evolution model. This is achieved following an iterative process designed to reach a convergence with respect to a defined matching condition, and consists of five key steps:

1. The user selects a binary evolution model and SFH;
2. Based on the SFH and the chosen initial parameter distribution, an initial population is generated;
3. The population evolves for a user specified number of steps, according to the selected evolution model;
4. If it is the first iteration, half of the simulated systems is compared with the total population. In the following steps, the population from the previous one gets compared to the population containing both the current and previous iterations. In any case, the comparison is done in order to check if the matching condition has been achieved;
5. Once the parameter distributions of the population have converged, the corresponding population is called *fixed population*, which represents the statistical features of a binary evolution model.

In practice, the fixed population is the converged, computationally efficient representation of the systems that we want to simulate, embedded in a complete small-scale synthetic galaxy that also contains other stellar components. The output is stored in a data frame, which separates the full galaxy properties from the fixed population ones. The last step required to construct a full size galaxy is to scale the fixed population (by mass or by number of stars) with a re-sampling approach with replacement, allowing to extrapolate a larger final population that preserves the statistical properties encoded in the fixed population.

[1] `https://cosmic-popsynth.github.io/docs/stable/pages/about.html`

[2] Note that, from now on, every time we talk about sampling, that is where the "M" of COSMIC comes into play: this code uses proficiently the Monte Carlo Markov Chain methods to sample populations and parameter distributions, as will follow in this section.

Initialization

The fixed population is generated from an initial collection of binaries sampled from distribution functions to assign to each binary an initial value of metallicity (Z), primary star mass (m), mass ratio (q), orbital separation (a), eccentricity (e), and birth time (T_0) according to the selected SFH. In COSMIC the user can choose between different binary parameter distributions, and different parameters can be treated independently. Moreover, COSMIC allows a complete personalization of the initial population through a number of other parameters, including different time-steps to control the binary physics, metallicity, stellar winds, common envelope phase, natal kicks, remnant mass, remnant spin, gravitational wave orbital decay, mass transfer, tides, and particular specifications for different kinds of stellar objects, mixing variables, and magnetic braking. In this work all the parameters were left default, but one: we tweaked the metallicity value, in order to differentiate fixed populations describing the parameter distributions for galaxies of different types. We will go more into detail on this topic in the next chapters.

Convergence

The number of simulated systems in the fixed population ideally describes the final parameter distribution functions while being low enough to keep the code efficient. Since every population depends on a different binary evolution model, to quantify this number a *discrete match criteria* is developed, based on the work Chatziioannou et al. [2017]. Independently generated histograms for each parameter are used to track their distribution as successive populations are generated and cumulatively added to the fixed population. The physical limits of the simulated systems are then enforced by taking the logistic transform, and finally the match is defined as:

$$match = \frac{\sum_{k=1}^{N} P_{k,i} P_{k,i+1}}{\sqrt{\sum_{k=1}^{N} (P_{k,i} P_{k,i}) \sum_{k=1}^{N} (P_{k,i} P_{k,i+1})}}, u$$

where $P_{k,i}$ is the probability for the kth bin, for the ith iteration. For how it is defined, the match value shifts between 0 and 1, and tends to unity as the parameter distributions converge to a distinct shape.

The output

Since COSMIC uses BSE as it's core binary evolution algorithm, the output of COSMIC follows most of the same conventions as BSE. The *kstar values* (e.g. the number that represent a specific stellar type) and evolution stages are nearly identical to their BSE counterparts, and the exact references can be found in the **Appendix**. In order to generate a fixed population, the COSMIC can be ran through a one-line command directly on the terminal, specifying a parameter file, the kstar values for the primary and secondary star, the maximum number of systems to evolve, every how many systems to check in, in order to track the distributions of the parameters, and how many processors to use. The final output is in an *hdf5* file containing several data frames, that keep track pf various important quantities during the evolution: the total number of stars and total mass of the entire population, the number of binaries, the convergence, and so on. The *conv* data frame contains all the information about the final fixed population, and thus is the one that we will use the most: from it we can extract all the parameter distributions of the fixed population, such as the orbital parameters, and the individual star information. The parameter distributions of a fixed population of binary white dwarfs with a default metallicity value set at 0.020 is shown in **Figure 2.2**.

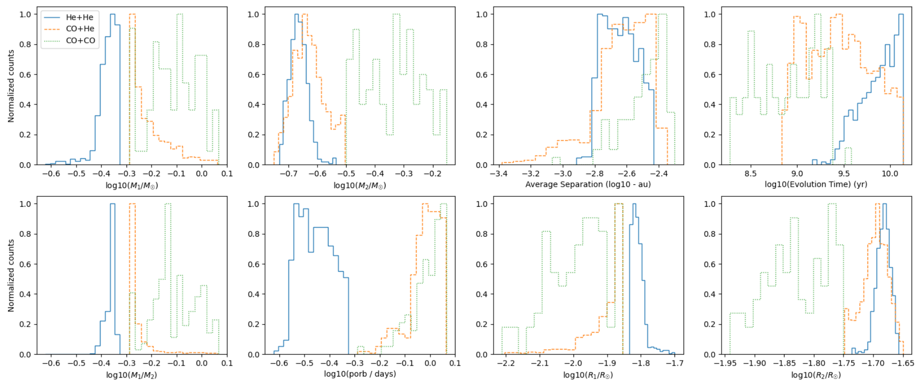

Figura 2.2: Distributions of the parameters of a fixed population with metallicity $Z = 0.020$ composed of He+He, CO+He and CO+CO binary white dwarfs. This includes the mass, radius of primary and secondary stars, the radius ratios between the two, the orbital period, average separation, and evolution time.

2.2.2 Astrophysical population

Once the convergence criteria is achieved, an astrophysical population can be sampled. The number of sources in the astrophysical population $N_{astro,tot}$ can be found by upscaling the size of the fixed population, N_{fixed} ,by the ratio of the mass of the astrophysical population, M_{astro}, to the mass of all the stars in the whole small-scale galaxy in which the fixed population is embedded, $M_{fixed,stars}$, as follows:

$$N_{astro} = N_{fixed} \frac{M_{astro,tot}}{M_{fixed,stars}}, \tag{2.1}$$

or by the ratio of the number of stars in the astrophysical population, $N_{astro,tot}$, to the total number of stars formed to produce the fixed population, $N_{fixed,tot}$,

$$N_{astro} = N_{fixed} \frac{N_{astro,tot}}{N_{fixed,stars}}. \tag{2.2}$$

Thus, to create a full-scale astrophysical population we need a *reference population* from which we can extract either the total mass or the total number of stars, to then use to scale up our fixed population. As we will now see, the chosen reference for our purpose is a catalog which reports many key galactic parameters in it, which will allow us to proceed using the method in (2.1).

2.3 GWGC and Galaxy Properties

As we have seen, the goal of this work is to simulate the gravitational wave background produced by compact binaries in the *local universe*, by generating the sources using COSMIC. To replicate the existing, observed galaxies in the vicinity of the Milky Way and simulate their stellar content we rely on the dataset provided in White et al. [2011], the **Gravitational Wave Galaxy Catalog** (GWGC). This catalog includes a list of $53,255$ galaxies within $100Mpc$ from earth, containing information on sky position, distance, blue magnitude, major and minor diameters, position angle, and galaxy type, currently used for follow-up searches of electromagnetic counterparts from gravitational wave searches.

2.3.1 What it has vs what we need

In principle, we could generate a separate fixed population for each galaxy in the GWGC and scale it individually. However, this is simply not practical because of the computational power and time it would require, and therefore we must find a strategy to group them in a few, representative, categories. As we will show in this section, many of the information in the GWGC can be used to infer the missing astrophysical quantities we need for population synthesis. Ultimately, we will find that metallicity is the most suitable parameter for grouping galaxies. To get there, we follow a chain of empirical relations, starting from the galaxy morphological type, through a luminosity to mass, and then a mass to metallicity relation. This process will enable us to provide COSMIC with the necessary input, found in a consistent and astrophysically motivated way.

2.3.2 Mass-luminosity relation

As previously discussed, in order to scale a fixed population to the size of a specific galaxy, we need either its total stellar mass or the number of stars. In particular, Faber and Gallagher [1979] presents a luminosity-to-mass relation that depends on the morphological type. This allows to use the blue magnitude and the T-type provided in GWGC to estimate each galaxy's stellar mass.

Magnitude to luminosity

To compute the stellar mass, the luminosity-to-mass ratio presented in Faber and Gallagher [1979] applies to the absolute blue luminosity of each galaxy. GWGC provides the absolute blue magnitude, thus we have to convert it into blue luminosity using the Sun's blue-band absolute magnitude as a reference (typically $M_{B,\odot} = 5.48$). Starting from the magnitude definition,

$$m_{B,gal} - m_{B,\odot} = -2.5 \log_1 0 \left(\frac{L_{B,gal}}{L_{B,\odot}} \right),$$

which, in stellar units, brings us to the following conversion:

$$L_{B,gal} = 10^{-0.4(m_{B,gal} - m_{B,\odot})} L_{B,\odot} \tag{2.3}$$

where $m_{B,gal}$ and $m_{B,\odot} \approx 5.48$ are the absolute blue magnitudes of the specific galaxy and the sun.

Galaxy morphological types

Although the GWGC denotes galaxy morphology using the de Vaucouleurs T-type scale, the luminosity-to-mass relations used in Faber and Gallagher [1979] are defined in terms of Hubble morphological classes. This classification is crucial because different morphological types exhibit significantly different stellar populations and star formation histories, which affect both luminosity and mass content. For example, elliptical galaxies generally have lower luminosity-to-mass ratios than spirals due to their older stellar populations and lack of ongoing star formation. Fortunately, a direct correspondence exists between T-type values and Hubble types, and thanks to the results in Faber and Gallagher [1979] we find the following correspondences:

T-Value	Hubble Class	$\frac{M}{L_B}$
−6.00 to −4.01	E	8.5
−4.00 to −2.01	$S0^-$	9.5
−2.00 to −0.99	$S0^+ - S_a$	6.2
1.00 to 3.99	$S_{ab} - S_{bc}$	6.5
4.00 to 4.99	$S_{bc} - S_c$	4.7
5.00 to 5.99	$S_{cd} - S_d$	3.9
6.00 to 10.00	$S_{dm} - Irr$	8.5

Tabella 2.1: WRITE CAPTION

The luminosity resulting from (2.3), expressed in units of solar blue luminosity $L_{B,\odot}$,

can then be multiplied by the appropriate M/L_B ratio, as in **Table 2.1**, to yield the total stellar mass for the galaxy

$$M_{gal} = \frac{M}{L_B} L_{B,gal} \tag{2.4}$$

2.3.3 Mass-metallicity relation

Now that we have estimated the stellar mass of each galaxy, we can also derive the corresponding metallicity. This is made possible by the results of Tremonti et al. [2004], where an empirical relation between stellar mass and gas-phase oxygen abundance (a proxy for galaxy metallicity) is established. The study, based on a sample of over 50,000 star-forming galaxies observed by the Sloan Digital Sky Survey, reveals a tight correlation between stellar mass and metallicity, spanning three orders of magnitude in mass and a factor of ten in metallicity, which can be written as follows:

$$Z' = -1.492 + 1.847 \times \log(M_*) - 0.08026 \times [\log(M_*)]^2, \tag{2.5}$$

where M_* is the galactic stellar mass, and

$$Z' = 12 + \log(O/H) \tag{2.6}$$

is the metallicity written in terms of the oxygen abundance (all the metallicity values with an apostrophe are intended as in these units).

On metallicity units

Now, in these units the sun's metallicity is[3] $Z'_\odot = 8.69$, whereas in the units used by COSMIC it is[4] $Z_\odot = 0.0134$ (all the metallicity values without the apostrophe are intended as in these units). We can easily find a conversion between the two unit systems by assuming that the rate of oxygen abundance in the galaxy and the one in the sun is equal to the rate of the metallicities in COSMIC's units,

$$\frac{(O/H)_{gal}}{(O/H)_\odot} = \frac{Z_{gal}}{Z_\odot}, \tag{2.7}$$

where (O/H) can be found inverting (2.6). At this point, knowing that $Z'_\odot = 8.69$, we can:

- Compute the Z'_{gal} value for each galaxy in GWGC using (2.5);
- Write $(O/H)_\odot$ and $(O/H)_{gal}$ in terms of the corresponding Z' value using (2.6): $(O/H) = 10^{(Z'-12)}$ and $(O/H)\odot \approx 0.32$.

Finally, finding Z_{gal} from (2.7), we can write the metallicity units conversion as:

$$Z_{gal} = 27.3 \times 10^{(Z'-12)}, \tag{2.8}$$

where the "27.3" coefficient mainly depends on the $Z_\odot$ value. This relation allows us to assign a realistic metallicity estimate to each GWGC galaxy in COSMIC's units, which we can now use to group them into representative subsets. This way, we can account for the significant impact of metallicity on stellar wind strength, remnant masses, and binary evolution outcomes, that greatly affects the expected gravitational wave signal.

2.3.4 Missing galaxies

The GWGC is far from being a complete list of the galaxies in the local Universe. As we will now see, there are two main factors contributing to this incompleteness: observational limitations due to the Zone of Avoidance (ZOA) and limitations of the information that the catalog presents.

Zone of avoiance

Since the GWGC is an observation-based catalog compiled from optical surveys, we must account for the Zone of Avoidance — the region of the sky obscured by the Milky Way's interstellar dust and stellar crowding, which impedes the detection of background galaxies. The extent of the ZOA depends on the wavelength of observation: infrared surveys penetrate deeper through the dust, while optical surveys, like those used for GWGC, are more strongly affected. In the optical band, the ZOA is expected to cover about $\sim 25\%$ of the sky Kraan-Korteweg and Lahav [2000]. For this work, we estimated the ZOA directly from the spatial distribution of galaxies in GWGC, by plotting their positions in Galactic coordinates. This way, the ZOA appears clearly as a horizontal band centered around the Galactic plane (see **Figure 2.3**). To quantify its extent, we

[3]This value is taken from the work Allende Prieto et al. [2001]
[4]This refers to the work Asplund et al. [2009]

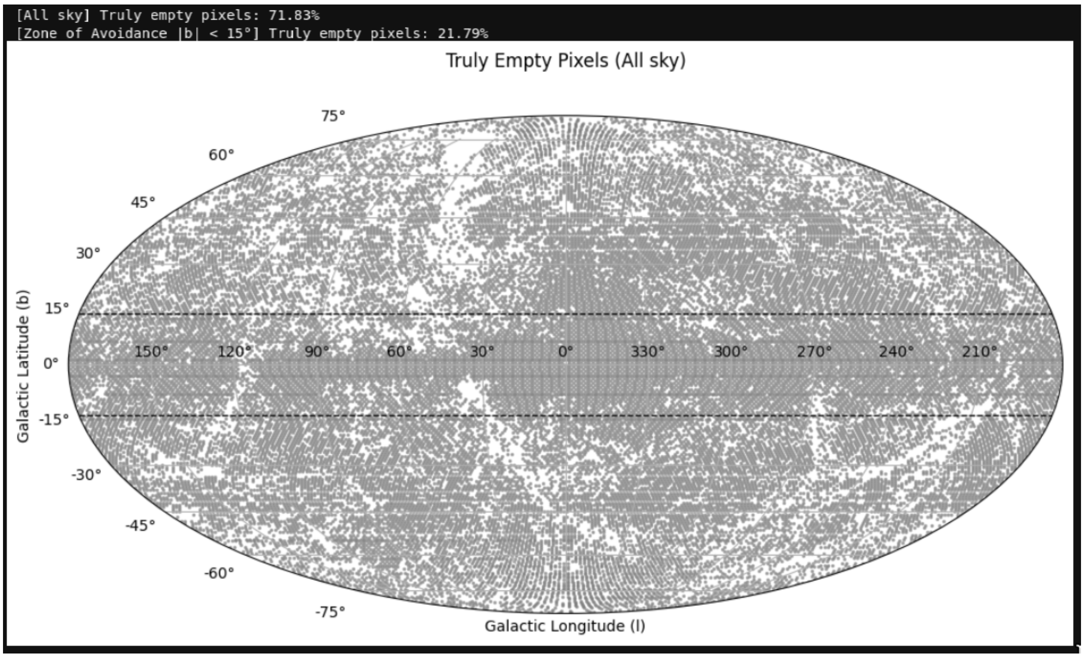

Figura 2.3: INSERT CAPTION AND REDO IMAGE IN PDF!!!

divided the sky map into n_{pix} equal-area pixels and focused on the band $|b| \leq 15^\circ$ in Galactic latitude. Counting the empty pixels in this band and dividing by n_{pix} gives an estimated ZOA coverage of $\sim$ 20%–25% of the sky, depending on the chosen pixel resolution. This estimate is fully consistent with the literature Kraan-Korteweg and Lahav [2000], so in our analysis we will assume that GWGC effectively covers $\sim$ 80% of the sky.

Incompleteness and non-galactic objects

Secondly, the entries of the GWGC represent a source of incompleteness themselves. Not all the objects listed in the GWGC are suitable for our purposes: in addition to galaxies, the catalog also includes globular clusters, which can be identified through their T-type values; moreover, not all galaxies in the catalog contain all the information required to perform the procedures described in the previous sections. To construct a working sample, we applied a series of masks to clean the catalog:

- Only keep entries classified as galaxies;
- Require that the distance, T-type, and absolute blue magnitude are provided;

After this selection, the sample we are left with reduced from the original $53,255$ entries to roughly $20,000$ galaxies suitable for population synthesis.

Filling the gap

In order to compensate the missing galaxies, we have make two physically motivated assumptions.

1. **Cosmological Principle:**
   The GWGC lists all the observed galaxies within $100Mpc$. On such scales, the Universe can be assumed to be statistically *homogeneous* and *isotropic*. This assumption is supported from observations of the *Cosmic Microwave Background* (CMB), where we know that the correlation function of the temperature fluctuations across the sky peaks at scales of $\sim 100Mpc$. Under this assumption, the selected galaxies of the GWGC should be statistically representative of the overall population in he same volume.

2. **Distance Matters:**
   The angular position is irrelevant in the computation of the gravitational wave signal; only the distance of the source matters. Therefore, missing galaxies from the unexplored volume covered by the Milky Way can be statistically represented by the galaxies from our retained sample.

Following these assumptions, we "fill in" the missing fraction of the sky and the dropped entries of the catalog by sampling with replacement from the cleaned GWGC, just like we did to extract an astrophysical from the fixed one, preserving its parameter distributions. This ensures that the statistical properties of the synthetic galaxy distribution match those of the observed portion while restoring the full-sky coverage. This is shown in a graphical representation of the distributions of distances, blue band magnitudes and T-types, in **Figure 2.4**: the distributions have been scaled up without visible changes.

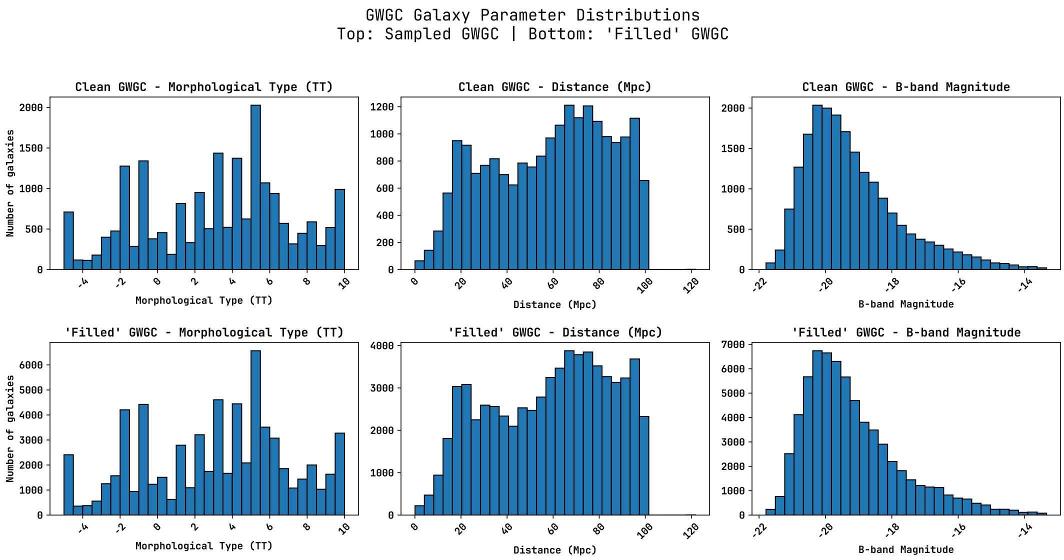

Figura 2.4: INSERT CAPTION

2.4 Final steps

Now that the catalog has been completed and its ready for the population synthesis, its time to put all the pieces together. We will analyze the metallicity distribution of the galaxies in the final catalog, categorize and generate the fixed populations accordingly, and make some final considerations regarding LISA's frequency resolution, how to take care of it, and how to sum gravitational wave signals of multiple sources that LISA will not be able to distinguish.

2.4.1 The final fixed populations

As we already discussed, the metallicity of a galaxy has a great impact on the stellar evolution and, thus, gravitational wave signal. This, plus the fact that metallicity is closely linked to the galaxy types too, led us to choose it as characterizing parameter for the populations that we will generate to represent the galaxy in the catalog. In particular, we the final catalog covers a range from a minimum of $Z = 0.00748$ to a maximum of $Z = 0.03948$. We decided to group all the values in between in ten equally wide bins, represented in **Figure 2.5**.

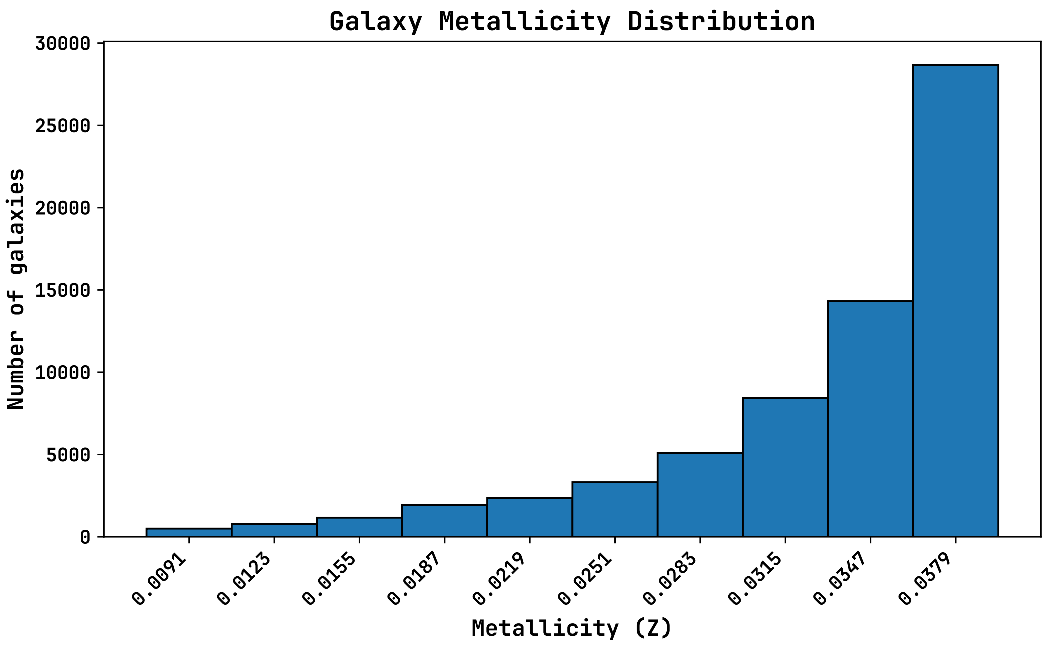

Figura 2.5: insert caption

Each one of the center values of the bins, shown in the x label, is linked to a different synthetic fixed population generated with COSMIC. For this thesis project, the fixed populations we generated covered the kstar values 10, 11 and 12, corresponding to He, CO, and Ne white dwarfs[5]. The simulation was done using ASK WILL INFO ON COSMIC-POP COMMAND USED.

2.4.2 LISA's frequency resolution

The duration of LISA's mission directly impacts its frequency resolution: the longer the observation time, the finer the frequency bins it can resolve. In this work, we assume

[5]INSERISCI TABELLA IN APPENDICE, E QUI IL RIERIMENTO

an observation tipe of:

$$T_{obs} = 4yr = 126, 144, 000s$$

which corresponds to a minimum frequency resolution of

$$\delta\nu_{LISA,min} \approx \frac{1}{T_{obs}} \sim 8 \times 10^{-9} Hz. \tag{2.9}$$

This fundamental limit comes from the Furier transform properties, and determines the smallest frequency interval over which the signals can be resolved. Although this is a very fine resolution, the precision of the orbital period in the simulated binary systems, and thus the frequency resolution on their gravitational signal, is actually much bigger, since these values come from a simulation rather than from real observations. For this reason, when computing the gravitational wave signals of our simulated binaries, we must take into account the fact that LISA will not be able to distinguish sources whose sources fall in the same frequency bin. To model this, we group the resulting gravitational wave signals in bins of size $\delta\nu_{LISA,min}$, and sum all the signals that fall within each bin, as we will now explain.

Multiple signals summation

To accurately represent the frequency resolution limit imposed by LISA's observation time, we have to sum all the signals within the same frequency bin. In principle, over the observation time T_{obs}, the orbital parameters of the sources may slowly evolve, causing a drift in the gravitational wave frequency. Integrating the resulting signal during this period is no easy task. However, for the slowly evolving white dwarf binaries we are considering, the change in such short time-frames is negligible, so we can treat their signals as effectively monochromatic within the observation window. Thus, we can define a commonly used variable to simplify our job, which is called **Amplitude Spectral Density** (**ASD**):

$$ASD = h\sqrt{T_{obs}}, \tag{2.10}$$

where h is the gravitational wave strain of the binary, computed in (??), and T_{obs} is the mission duration for LISA. This quantity represents the characteristic strain amplitude of the gravitational wave signal per square root of frequency, scaled by the observation time, and its very convenient for comparing the signals in frequency space. Correspondingly, we can define the **Power Spectral Density** (**PSD**) as the square of the ASD

$$PSD = ASD^2, \tag{2.11}$$

which properly represents the signal power per frequency unit. Since power contributions from independent sources add linearly, the total PSD in a given frequency bin is simply found by summing the power of all the sources within it:

$$PSD_{tot,bin_1} = PSD_{1,bin_1} + PSD_{2,bin_1} + \dots \tag{2.12}$$

This way, we effectively accounted for LISA's frequency resolution limit. The reason for introducing this quantities is that gravitational waves from different binaries are uncorrelated, so their strains add incoherently. This means we cannot simply sum the strain amplitudes directly. Instead, the PSD provides a way to combine signals that ensures a correct representation of the combined gravitational wave background.

Capitolo 3

Results

The signal computation

At this point we are fully equipped to be able to compute the gravitational wave signal of the sources. This will be done in an iterative process applied to each galaxy in the final catalog, which consists of the following steps:

- Compute the right N_{astro} using the (2.1)
- Scale the fixed population accordingly, thus creating the full-scale galaxy simulation. At this point for each binary system in this astrophysical population we:
  - Compute each binary's gravitational wave signal using (??)[1];
  - Bin this signal to LISA's frequency bins, by summing it using (??);
  - Plot this value on LISA's curve.

- Plot of spectral distribution of the computed signal - Analysis of the distribution of the sources - Eventual implications (none, since it shouldn't be visible)

[1]Note here that all the binaries within the same galaxy are given the same distance from us. This approximation is valid since the distance of the galaxy is much much bigger the its size, and thus the maximum possible distance between tow binaries within the same galaxy.

Capitolo 4

Conclusions and Future Perspectives

Recap of the whole Work - Limits of the Work, assumptions and approximations used - Possible extensions

Appendice A

Appendix

Dettagli tecnici sul codice.

Tabelle di parametri.

Ulteriori grafici.

Script di calcolo, se rilevante.

INSERISCI TABELLE COI KSTAR VALUES ETC

Bibliografia

Carlos Allende Prieto, David L. Lambert, and Martin Asplund. The Forbidden Abundance of Oxygen in the Sun. ApJ, 556(1):L63–L66, July 2001. doi: 10.1086/322874.

Martin Asplund, Nicolas Grevesse, A. Jacques Sauval, and Pat Scott. The Chemical Composition of the Sun. ARA&A, 47(1):481–522, September 2009. doi: 10.1146/annurev.astro.46.060407.145222.

Katelyn Breivik, Scott Coughlin, Michael Zevin, Carl L. Rodriguez, Kyle Kremer, Claire S. Ye, Jeff J. Andrews, Michael Kurkowski, Matthew C. Digman, Shane L. Larson, and Frederic A. Rasio. COSMIC Variance in Binary Population Synthesis. ApJ, 898(1):71, July 2020. doi: 10.3847/1538-4357/ab9d85.

Katerina Chatziioannou, James Alexander Clark, Andreas Bauswein, Margaret Millhouse, Tyson B. Littenberg, and Neil Cornish. Inferring the post-merger gravitational wave emission from binary neutron star coalescences. Phys. Rev. D, 96(12):124035, December 2017. doi: 10.1103/PhysRevD.96.124035.

S. E. de Mink, O. R. Pols, and R. W. Hilditch. Efficiency of mass transfer in massive close binaries. Tests from double-lined eclipsing binaries in the SMC. A&A, 467(3): 1181–1196, June 2007. doi: 10.1051/0004-6361:20067007.

Michal Dominik, Krzysztof Belczynski, Christopher Fryer, Daniel E. Holz, Emanuele Berti, Tomasz Bulik, Ilya Mandel, and Richard O'Shaughnessy. Double Compact Objects. I. The Significance of the Common Envelope on Merger Rates. ApJ, 759 (1):52, November 2012. doi: 10.1088/0004-637X/759/1/52.

S. M. Faber and J. S. Gallagher. Masses and mass-to-light ratios of galaxies. ARA&A, 17:135–187, January 1979. doi: 10.1146/annurev.aa.17.090179.001031.

Aaron M. Geller, Nathan W. C. Leigh, Mirek Giersz, Kyle Kremer, and Frederic A. Rasio. In Search of the Thermal Eccentricity Distribution. ApJ, 872(2):165, February 2019. doi: 10.3847/1538-4357/ab0214.

D. Goldberg and T. Mazeh. The mass-ratio distribution of the spectroscopic binaries in the Pleiades. A&A, 282:801–803, February 1994.

D. C. Heggie. Binary evolution in stellar dynamics. MNRAS, 173:729–787, December 1975. doi: 10.1093/mnras/173.3.729.

Jarrod R. Hurley, Onno R. Pols, and Christopher A. Tout. Comprehensive analytic formulae for stellar evolution as a function of mass and metallicity. MNRAS, 315(3): 543–569, July 2000. doi: 10.1046/j.1365-8711.2000.03426.x.

Jarrod R. Hurley, Christopher A. Tout, and Onno R. Pols. Evolution of binary stars and the effect of tides on binary populations. MNRAS, 329(4):897–928, February 2002. doi: 10.1046/j.1365-8711.2002.05038.x.

J. Klencki, M. Moe, W. Gladysz, M. Chruslinska, D. E. Holz, and K. Belczynski. Impact of inter-correlated initial binary parameters on double black hole and neutron star mergers. A&A, 619:A77, November 2018. doi: 10.1051/0004-6361/201833025.

Renée C. Kraan-Korteweg and Ofer Lahav. The Universe behind the Milky Way. A&A Rev., 10(3):211–261, January 2000. doi: 10.1007/s001590000011.

Pavel Kroupa. On the variation of the initial mass function. MNRAS, 322(2):231–246, April 2001. doi: 10.1046/j.1365-8711.2001.04022.x.

Pavel Kroupa, Christopher A. Tout, and Gerard Gilmore. The Distribution of Low-Mass Stars in the Galactic Disc. MNRAS, 262:545–587, June 1993. doi: 10.1093/mnras/262.3.545.

Tsevi Mazeh, Dorit Goldberg, Antoine Duquennoy, and Michel Mayor. On the Mass-Ratio Distribution of Spectroscopic Binaries with Solar-Type Primaries. ApJ, 401: 265, December 1992. doi: 10.1086/172058.

Maxwell Moe and Rosanne Di Stefano. Mind Your Ps and Qs: The Interrelation between Period (P) and Mass-ratio (Q) Distributions of Binary Stars. ApJS, 230(2):15, June 2017. doi: 10.3847/1538-4365/aa6fb6.

Edwin E. Salpeter. The Luminosity Function and Stellar Evolution. ApJ, 121:161, January 1955. doi: 10.1086/145971.

Christy A. Tremonti, Timothy M. Heckman, Guinevere Kauffmann, Jarle Brinchmann, Stéphane Charlot, Simon D. M. White, Mark Seibert, Eric W. Peng, David J. Schlegel, Alan Uomoto, Masataka Fukugita, and Jon Brinkmann. The Origin of the Mass-Metallicity Relation: Insights from 53,000 Star-forming Galaxies in the Sloan Digital Sky Survey. ApJ, 613(2):898–913, October 2004. doi: 10.1086/423264.

L. M. van Haaften, G. Nelemans, R. Voss, S. Toonen , S. F. Portegies Zwart, L. R. Yungelson, and M. V. van der Sluys. Population synthesis of ultracompact X-ray binaries in the Galactic bulge. A&A, 552:A69, April 2013. doi: 10.1051/0004-6361/201220552.

Darren J White, E J Daw, and V S Dhillon. A list of galaxies for gravitational wave searches. *Classical and Quantum Gravity*, 28(8):085016, March 2011. ISSN 1361-6382. doi: 10.1088/0264-9381/28/8/085016. URL `http://dx.doi.org/10.1088/0264-9381/28/8/085016`.